

Article

Method for Measuring Interface Pressure of High-Voltage Cables

Chao Lyu ¹, Shuang Wang ¹, Shuang Liu ^{1,*} and Yi Guo ^{2,*}

¹ College of Engineering Science and Technology, Shanghai Ocean University, Shanghai 201306, China; clv@shou.edu.cn (C.L.); wangs199610@163.com (S.W.)

² Fisheries Bureau, Ministry of Agriculture and Rural Affairs, Beijing 100125, China

* Correspondence: s-liu@shou.edu.cn (S.L.); 13911268568@189.cn (Y.G.)

Abstract: In high-voltage cables, because of the close fit of their internal structures, interface pressure is generated between conductor and insulator, which affects the performance of the cable. Studies on the calculation and testing of the interfacial pressure of cable conductors are scarce because of the lack of a unified formula and the difficulty of direct measurement. As such, in this study, we devised two methods for calculating and measuring the interface pressure of cable conductors. In the first, we used two physical experimental methods. We used the friction between cable components to perform the calculation and create an experimental method for determining cable conductor interface pressure; on the basis of the equation of the pressure inside and outside a thick-walled cylinder using elasticity mechanics, we calculated the interface pressure on the basis of the measurement of the strain state of the inner and outer diameters of each layer of the cable under different assembly and stripping conditions. We verified the effectiveness of the methods through physical tests and simulations using a YJLW03 1 × 1200 high-voltage cable. Then, we used simulation software ANSYS and SolidWorks to calculate the interface pressure. With different simulation settings, we obtained results regarding interface pressure. Lastly, these simulated values were individually compared with two physical tests, and the error was calculated. Results obtained in the ANSYS environment showed that interface pressure values determined by the geometric interference normal stress, geometric interference pressure, contact interference normal stress, and contact interference pressure methods were 39.75, 36.84, 5.76, and 36.57 MPa, respectively. In SolidWorks software, we used the contact-stress and X-axis normal stress methods. Results were all 37.36 MPa. Then, simulation results and experimental results were compared, and error was calculated. The comparison showed that the X-axis orthogonal stress method was the most accurate. Errors between the X-axis orthogonal stress method and the two physical experiments were 1.5% and 0.48%. Through the above simulation and physical experiments, we determined the interface pressure between conductors and insulators in a high-voltage power cable. We obtained the cable interface pressure value through two kinds of physical experiments, and these two methods were clearly reliable. Simulation experiments showed that using SolidWorks software to simulate this problem obtained better results. Research results provide technical support and reference for the calculation and measurement of cable interface pressure and the optimization of cable performance.

Keywords: high-voltage cable; interface pressure; elastic mechanics; experimental simulation; finite element analysis



Citation: Lyu, C.; Wang, S.; Liu, S.; Guo, Y. Method for Measuring Interface Pressure of High-Voltage Cables. *Electronics* **2022**, *11*, 1419. <https://doi.org/10.3390/electronics11091419>

Academic Editors: Albert Smalcerz and Marcin Blachnik

Received: 12 February 2022

Accepted: 25 April 2022

Published: 28 April 2022

Publisher's Note: MDPI stays neutral with regard to jurisdictional claims in published maps and institutional affiliations.



Copyright: © 2022 by the authors. Licensee MDPI, Basel, Switzerland. This article is an open access article distributed under the terms and conditions of the Creative Commons Attribution (CC BY) license (<https://creativecommons.org/licenses/by/4.0/>).

1. Introduction

A cable is a device used for electrical energy or signal transmission, usually composed of several wires or groups of wires. A power cable is a cable product used to transmit and distribute high-power electrical energy in the main line of a power system, including voltage levels of 1–500 kV and higher. Power cables have been used for more than a century [1]. As such, research on the mechanical analysis of wires and cables covers many aspects.

The force characteristics of conductors in power cables have been extensively studied. Lu et al. and Zhou et al. [2,3] established two finite-element models of steel core aluminum stranded wire in bending and tension states, and analyzed the tension effect on the wire. Extension tests verified the accuracy of the models. Then, the effect of stress in the intermediate joint of the cable on the cable accessories and conductors was studied. Yi et al. [4] used a superelastic model to calculate mechanical stress distribution in a cable accessory, a rubber stress cone. Among cable accessories produced in China, cold shrink cable glands are the most commonly used, and the utilization rate is as high as 90%. Chen [5] used a sensor to measure the interface pressure of a cable joint. Jia [6] constructed a theoretical calculation model for the interface structure, deduced the theoretical calculation of the interface pressure of cold shrinkable intermediate joints, and verified the model through experiments. Qiu [7] explored the influence of the intermediate joint on the interface pressure in the bending state. In addition to cold-shrinkable joints, Tian [8,9] used finite-element calculation and test methods to analyze changes in interface pressure before and after the installation of prefabricated cable joints. He also studied the changes in Young's modulus and the interface pressure of different joint materials.

The interface pressure between cable conductor and insulator was also studied. Zhang [10] designed an interface pressure test device for rubber parts using a thin-walled aluminum tube with the same outer diameter as the cable to replace the actual cable. The author of that study placed strain gauges inside the tube and measured the inner shell wall by electrical measurement when the rubber part was loaded as the dependent variable.

The influence of other cable factors on cable performance was studied. In terms of thermal stress research of cable joints, Hamdan and Raffaella [11,12] studied the interface pressure changes of cable joints under different temperature conditions and thermal cycles. In addition, different cable insulation aging conditions of the cable layer influence the interface pressure of the joint [13], with a study conducted on the resistance of the cable network during the installation process [14].

The interface pressure between cable body and cable accessories determines the electrical strength of the interface. If interface pressure is too low, the electrical strength requirements of the accessories are not met. If the interface pressure is too high, it causes an interference fit of the contact part and damages the cable accessories. Interface pressure between cable body and cable accessories is key to ensuring the safe operation of cable accessories [15]. As such, in this study, we focused on the interface pressure between cable conductor and insulator.

Research on the mechanical properties of wire conductors in various states and on the interface pressure of cable joints has advanced, but studies on the interface pressure of cable conductors are lacking. Due to the tight fit of the cable because of the interference fit, interface pressure is generated between layers. Insufficient interface pressure between stress cone and cable insulation may cause the cable terminal to malfunction [16], but no formula is available for calculating the interface pressure between cable conductor and insulator, and directly measuring it with the sensor method is difficult. For this reason, a practical method for calculating and measuring the interface pressure of cable conductors is needed to provide technical support for the optimization of cable performance.

To calculate and measure the interface pressure on a cable conductor, we designed two experimental methods for measuring the interface pressure of the cable conductor. The first method (Experiment 1) involves using the tensile test of the cable conductor to determine the interface pressure of the cable conductor by measuring the friction force between cable components. The second experiment (Experiment 2) utilizes the principle of elasticity. Interfacial pressure is calculated by measuring the change in the inner and outer diameters of each cable layer before and after stripping. Then, we designed a method on the basis of a combination of simulation and physical experiments to validate the results.

We proved the effectiveness of the physical experimental method proposed in this paper to calculate interface pressure through physical experiments and finite-element analysis methods, and found that the methods of Experiments 1 and 2 are even suitable for

cables with different voltage levels and research objects. Here, we propose an innovative interface pressure calculation method.

2. Materials and Methods

2.1. The Literature and Research Structure

2.1.1. The Literature

Research on cables can be divided into various categories: cable conductors and their terminals [17–22], cable accessories [23–25], cable insulators and their aging, water trees, electrical trees [26–28], power-cable fault monitoring [29–33], and submarine cables [34–36].

Research objects and methods in the literature differed over time. In this study, we focused on the interfacial pressure between cable conductor and insulator, which is rarely studied. We performed physical experiments and simulation analysis, devised two methods to measure the interface pressure, and obtained data through an experiment. We then compared experimental and simulation results, from which we produced a conventional method to study the interface pressure of conductors. We verified the two methods through physical experiments in this study for both conductors and other types of cables in this experiment. Related studies in the literature [17–36] are summarized in Table 1.

Table 1. Study summary.

Category	References	Main Methods and Brief Content
Cable conductor and its terminal [17–22]	Yu, Z. (2021) T., L.B. (2018) Haijun, Z. (2021) Lihua, Z. (2021) Liao, Y. (2020) Danqi, Li (2019)	Designs or calculates research objects through physical formula derivation or simulation software
Problems with cable accessories [23–25]	Weiwei, L. (2021) Liang, H (2019) Xu, D.P (2020)	Isolates and correlates cable accessories
Cable insulator and its aging, water trees, and electric trees [26–28]	Sun, F. (2021) Ez, A. (2019) Hao, Y.A. (2021)	Uses existing aging cable insulation to analyze water and electric trees
Power cable fault monitoring [29–33]	Li, K. (2021) Xia, Z. (2021) Lai, Q. (2020) Zhu, C. (2019) Pompili, M. (2021)	Analyzes and propose new solutions and monitoring methods on the basis of known cable and power system faults
Submarine cables [34–36]	Ar, A. (2021) Viespoli, L.M. (2021) Yz, A. (2021)	Mainly based on actual working environments for analysis and calculation

2.1.2. Research Structure

First, we used formulas for friction force and elastic mechanics to construct two methods for calculating the interface pressure of a cable. Second, we designed physical experiments related to the formula derivation, and measured and calculated the relevant data. Third, we analyzed cable interface pressure values using ANSYS (Version 19.2, ANSYS, Pittsburgh, PA, USA) and SolidWorks (Version 2021, SolidWorks, Concord, MA, USA). Lastly, we compared and analyzed obtained values from the previous steps to draw our conclusions. The flowchart of our methodology is shown in Figure 1.

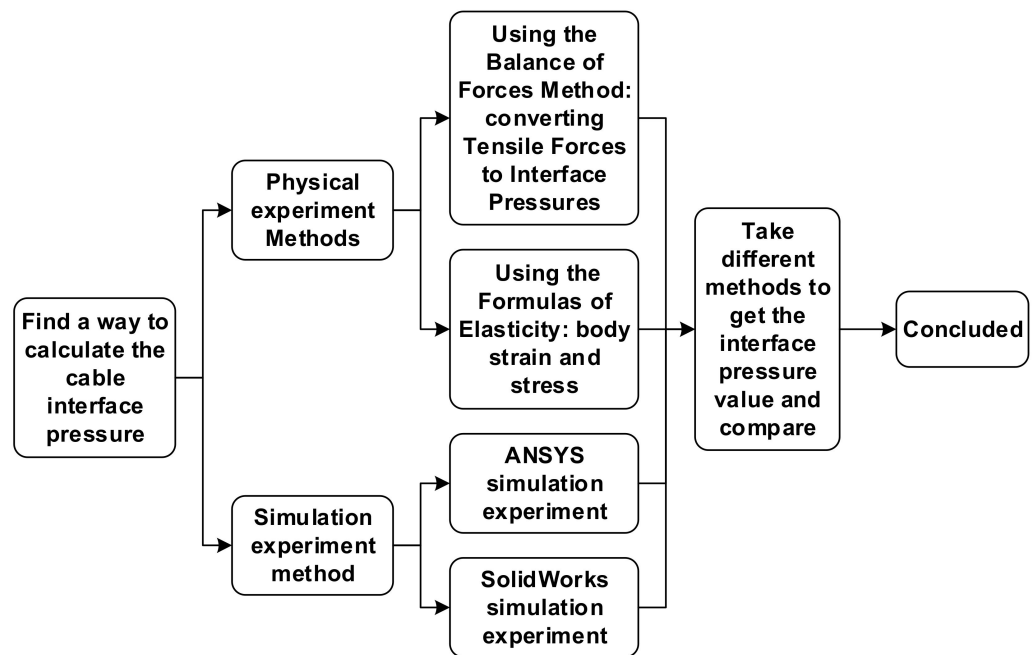


Figure 1. Study flowchart.

2.2. Structural and Material Composition of High-Voltage Cables

The basic structure of a power cable is composed of four parts: the core (conductor), insulating layer, shielding layer, and protective layer. The interior of a high-voltage cable is more complex, having a water-blocking layer and a protective asphalt layer. The sheath is composed of stronger materials. Figure 2 depicts a schematic diagram of the structure of a high-voltage cable. In this study, we used YJLW03 1 × 1200 (Shanghai Sanyuan Cable Accessories Co., Ltd., Shanghai, China) as a cable model, which is a power cable with cross-linked polyethylene insulation, a corrugated aluminum sheath, and a polyethylene outer sheath. Copper was the conductor, and the nominal cross-section was 1200 mm².

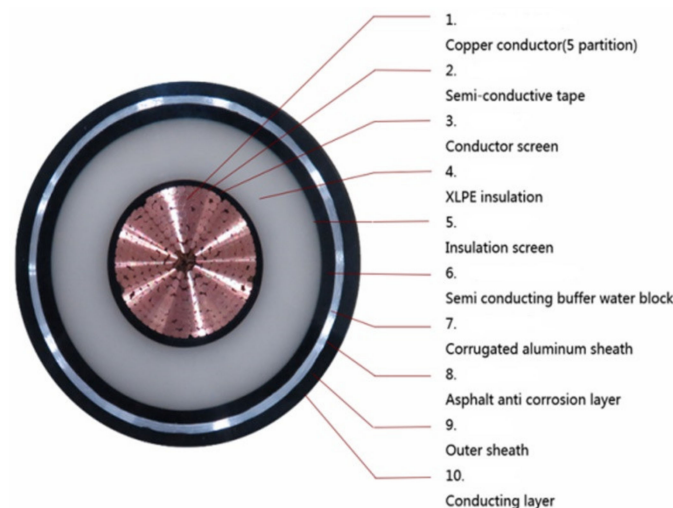


Figure 2. Cross-sectional model of high-voltage cable.

In high-voltage cables, the interface pressure between conductor and insulator refers to the interface pressure between XLPE (Cross linked polyethylene, Cable insulation materials) insulator and copper conductor. The direction of pressure points to the center of the cross-section of the conductor. Because the shielding and water-blocking layers were composed of thin and flexible materials, in this study, we simplified the cable model as a four-layer structure with a conductor, insulator, sheath, and outer sheath.

2.3. Theoretical Calculation Method for Interface Pressure

The conductor interface pressure is expressed as the compressive stress between copper conductor and cross-linked polyethylene insulating layer. Compressive stress can be calculated using two methods: the ratio of the positive pressure on the conductor to the contact area, and elasticity calculated by the method for solving plane problems in mechanics. Our study is based on these two methods, through which we analyzed and calculated the conductor interface pressure.

2.3.1. Positive Pressure Determines Interface Pressure

According to Coulomb's friction law, friction is proportional to the load (positive pressure), and the proportional coefficient is f . If directly measuring a load is difficult, the value of the load can be determined by the magnitude of the friction force as follows:

$$F = f \times p \quad (1)$$

where F is friction force, f is friction coefficient, and p is positive pressure.

A Cartesian coordinate system was established where x represents the direction of the cable axis, and y represents the direction perpendicular to the cable axis. Friction force F can be derived from the force balance equation. According to Newton's law of motion, in the state of static or uniform motion, the resultant external force on an object is zero. After the resultant external force is orthogonally decomposed, the resultant external forces in the x and y directions are zero, so the force in the x direction is:

$$F = \sum_{i=1}^n F_i \quad (i = 1, 2, 3 \dots n) \quad (2)$$

where F_i is force other than friction force in the x direction, and i represents force in each direction.

Combining Formulas (1) and (2), we obtain the value of positive pressure, and compressive stress can then be obtained from the stress calculation formula:

$$\sigma = \frac{p}{A} \quad (3)$$

where σ is compressive stress, which is interface pressure; p is load (positive pressure); and A is contact area.

2.3.2. Elastic Mechanics Formula Determines Interface Pressure

On the basis of the principle of elastic force [37,38], the internal and external pressure of the circular wall tube in the plane can be solved. Here, we provide some derivations based on the basic formulas of elastic mechanics.

1. Definition of thick- and thin-walled tubes

Thick- and thin-walled cylinders are usually defined as cylinders with a ratio of outer to inner diameter that is greater than 1.2, and cylinders with a ratio of wall thickness to outer diameter of less than 0.05, respectively:

$$\frac{a}{b} = k_1 > 1.2 \quad (4)$$

$$\frac{d}{a} = k_2 < 0.05 \quad (5)$$

where a is outer diameter, b is inner diameter, d is the thickness of the cylinder wall, and k_n ($n = 1, 2$) is the corresponding ratio that is defined as a thick-walled cylinder if it satisfies Formula (4).

2. Infinitesimal body decomposition of thick-walled cylinder

Suppose a thick-walled cylinder has external pressure p_1 , internal pressure p_2 , outer diameter a , and inner diameter b . Taking the center of the cross-section of the thick-walled tube as the z axis, the central angle of the counterclockwise arc as the θ axis, and the radius of the cross-section as the r axis, a cylindrical coordinate system can be established. We

then intercepted two cylindrical surfaces from r and $r + dr$. θ and $\theta + d\theta$ form two radial planes, and z and $z + dz$ cut two horizontal planes perpendicular to the z axis, as shown in Figure 3.

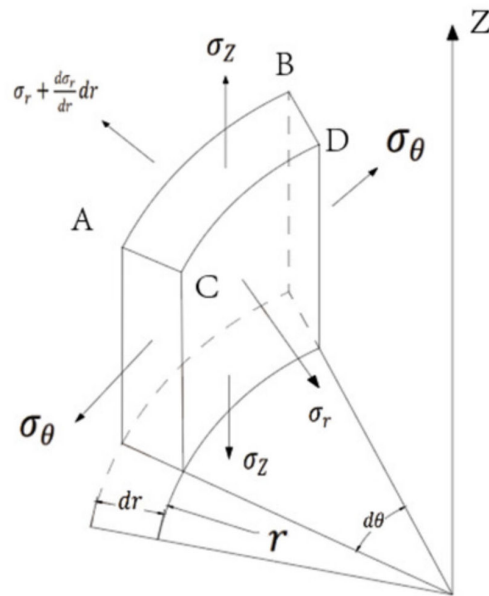


Figure 3. Three-dimensional microelement body of thick-walled cylinder.

3. Transforming three-dimensional microelement body into two-dimensional microelement body

Suppose that the displacement component in the r direction is u , and the component in the z direction is w . Normal stresses σ_r , σ_θ , and σ_z , and radial displacement u are all independent of θ and z . A three-dimensional microelement body can then be transformed into a two-dimensional microelement body, and the relevant planar polar coordinates are established as shown in Figure 4.

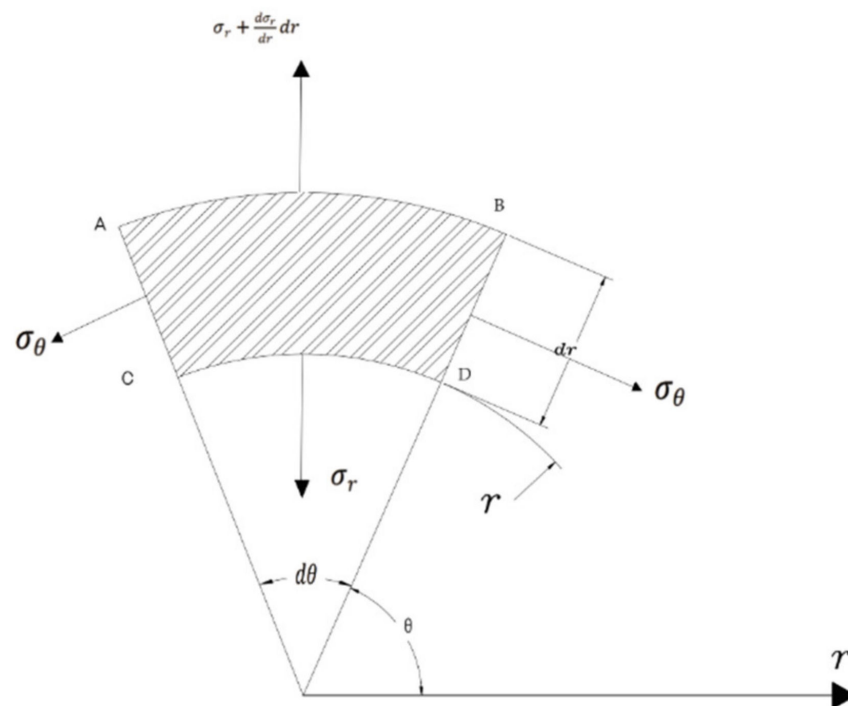


Figure 4. Two-dimensional microelement surface of thick-walled cylinder.

We established a balance equation along the radial direction and used boundary conditions

$$(\sigma_r)_{r=a} = -p_1 \quad (6)$$

$$(\sigma_r)_{r=b} = -p_2 \quad (7)$$

Lastly, we obtained:

$$\sigma_r = \frac{a^2 b^2}{b^2 - a^2} \frac{p_2 - p_1}{r^2} - \frac{a^2 p_1 - b^2 p_2}{b^2 - a^2} \quad (8)$$

$$\sigma_\theta = \frac{a^2 b^2}{b^2 - a^2} \frac{p_2 - p_1}{r^2} - \frac{a^2 p_2 - b^2 p_1}{b^2 - a^2} \quad (9)$$

In particular, when the external pressure of the wall cylinder is zero,

$$p_1 = 0 \quad (10)$$

We substituted (10) into (8) and (9) to obtain

$$\sigma_r = \frac{a^2 p_1}{b^2 - a^2} \left(1 - \frac{b^2}{r^2} \right) \quad (11)$$

$$\sigma_\theta = \frac{a^2 p_1}{b^2 - a^2} \left(1 + \frac{b^2}{r^2} \right) \quad (12)$$

Then, Formulas (8) and (9) are called the Lamé formulas.

Similarly, radial displacement u can be obtained by Formulas (8) and (9) to obtain:

$$u = \frac{1 - \nu}{E} \frac{(b^2 p_2 - a^2 p_1)}{a^2 - b^2} + \frac{1 + \nu}{E} \frac{a^2 b^2 (p_2 - p_1)}{(a^2 - b^2)r} \quad (13)$$

In Equation (13), a and b are the outer and inner diameters of a thick-walled cylinder, p_1 is the external pressure, p_2 is the internal pressure, E is the modulus of elasticity, and ν is Poisson's ratio. Internal and external pressure can be calculated according to the radial displacement, and the size of the internal and external diameters.

According to this formula, we obtained some results:

① Radial displacement u is related to internal and external pressure p_1 and p_2 , respectively, and to outer and inner diameters a and b , respectively. u is related to the basic physical parameters of the material.

② Internal pressure p_2 can be calculated according to this formula by measuring radial displacement u and external pressure p_1 .

2.4. Interface Pressure Measurement Experiment Scheme

According to the theoretical formula in Section 2, we designed a method for calculating and measuring cable interface pressure.

2.4.1. Cable Tension Test

On the basis of the physical principle mentioned in Section 2.3.1, we designed a physical experiment to find the interface pressure of a cable. In the cable pulling test (Experiment 1), we measured the required pulling force when the cable conductor is removed. According to the method in Section 2.3.1, the test results of Experiment 1 could be converted into the interface pressure between cable conductor and insulator. The tensile test device is shown in Figure 5a. Before the experiment started, the cable was placed into the model. At the beginning of the experiment, the pulling force was provided by a pulling machine, which slowly pulled the cable conductors out. The right side of the cable, displayed in Figure 5b, was the end used for the tensile test, which provided the tensile force required for the experiment. The left side was connected to a computer to display the tensile force value of the cable. Lastly, we determined the relationship between tensile force and elongation displacement.

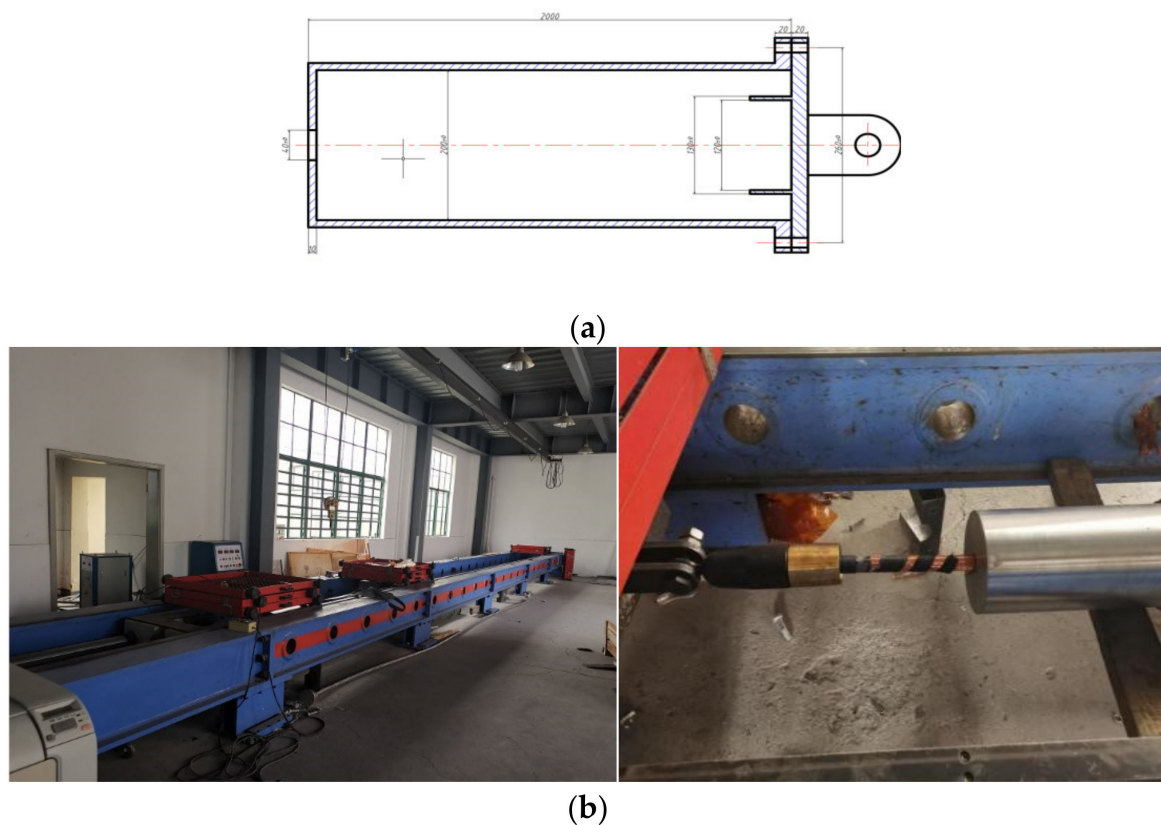


Figure 5. (a) Experimental tool (cable fixed inside before the experiment began). (b) Experimental fixture and mold, and tensile test conductor.

2.4.2. Cable Deformation Experiment

Due to the tight fit of the cables, elastic deformation occurs due to the interface pressure after the cable leaves the factory. After this elastic deformation, the cable can return to its original shape when compression is released. In the cable deformation experiment (Experiment 2), we used changes in the inner and outer diameters of the cable conductors under different stresses before and after stripping to determine the deformation value, and then calculated the deformation of each layer using Equations (6)–(13) in Section 2.3.2. External force on the outermost polyethylene sheath was zero, and the outer pressure of the inner layer was equal to the inner pressure of the outer layer in opposite directions. The experimental scheme is as follows:

1. Material preparation: Take a 20 cm long cable, which is the same as the above cable model, use a chainsaw to cut it into two halves, and mark the two parts obtained as Parts A and B.
2. Measurement: Use Vernier calipers to measure and record the inner and outer diameters of each material in part A.
3. Mean value processing: Because of cable technology and transportation reasons, the actual cable is not completely cylindrical, so the average value is used for multiple measurements.
4. Part B: Strip the cable structure at a time according to the number of layers from which the cable is produced. Remove the material of Part B according to the layers. Because the insulating layer composed of cross-linked polyethylene is hard and difficult to separate, it must be drawn out of the conductor.
5. Measure after the deformation is stable: After separating each material, leave the material in place for 24 h, and conduct measurements after it is stable. During the measurement, record multiple measurements and use the average value.

Pictures before and after processing are shown in Figure 6.

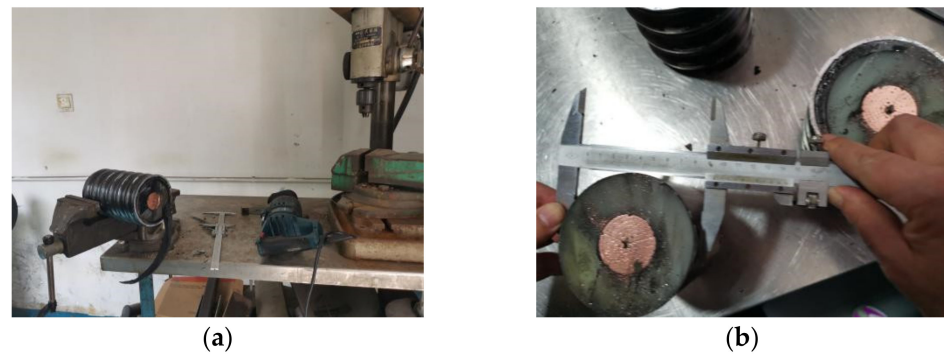


Figure 6. Experiment 2 processing diagram. (a) Part A and (b) Part B measuring stripped part.

2.5. Simulation Method

To further verify the validity of the analytical results and the reliability of the experimental method, we conducted simulation experiments using ANSYS Workbench 19.2 and SolidWorks simulation 2018 software. For the simulation, we used data obtained in Experiments 1 and 2. We built the cable models in both simulation software packages. We established different simulation models according to different software simulation methods. Lastly, we obtained simulation results for the cable interface pressure value.

2.5.1. ANSYS Workbench Simulation Experiment

The interface pressure on a cable conductor can be regarded to be pressure caused by the interference fit. The two methods used for simulating interference assembly in Workbench are geometric interference setting and the contact interference setting. The geometric interference method is used to create the interference fit in ANSYS Design Modeler, that is, the outer diameter radius value of the inner layer was set to be larger than that of the inner diameter radius value of the outer layer during modeling to achieve the interference effect. In the second method, geometric interference is not set in the modeling, but in the contact settings in the model by changing the contact interface adjustment option interface treatment and setting the offset value to set the interference.

In preprocessing, we used Design Modeler in ANSYS Workbench for modeling. When modeling, we ignored the conductor-shielding, insulating-shielding, and water-blocking layers. From the innermost to the outermost layer were the conductor, insulator, aluminum alloy sheath, and polyethylene outer sheath. We used the form of a quarter circle during modeling and added symmetry settings during preprocessing. The modeling is shown in Figure 7a,b. Figure 7c shows the different interferences of the two models. The comparison in Figure 7c shows that the geometric interference method had overlapping inner and outer diameters.

Geometric Interference Setting Method

The geometric interference setting creates the interference fit. When modeling, we set the outer diameter of the inner material to be slightly larger than the inner diameter of the outer material, so that the interference effect can be achieved. We built the model and divided the mesh as shown in Figure 8. We meshed the cable model, and the black line indicates the mesh division line, which creates small units.

Contact Interference Setting Method

In the contact interference setting, preprocessing does not use the geometric interference method to model and mesh the model.

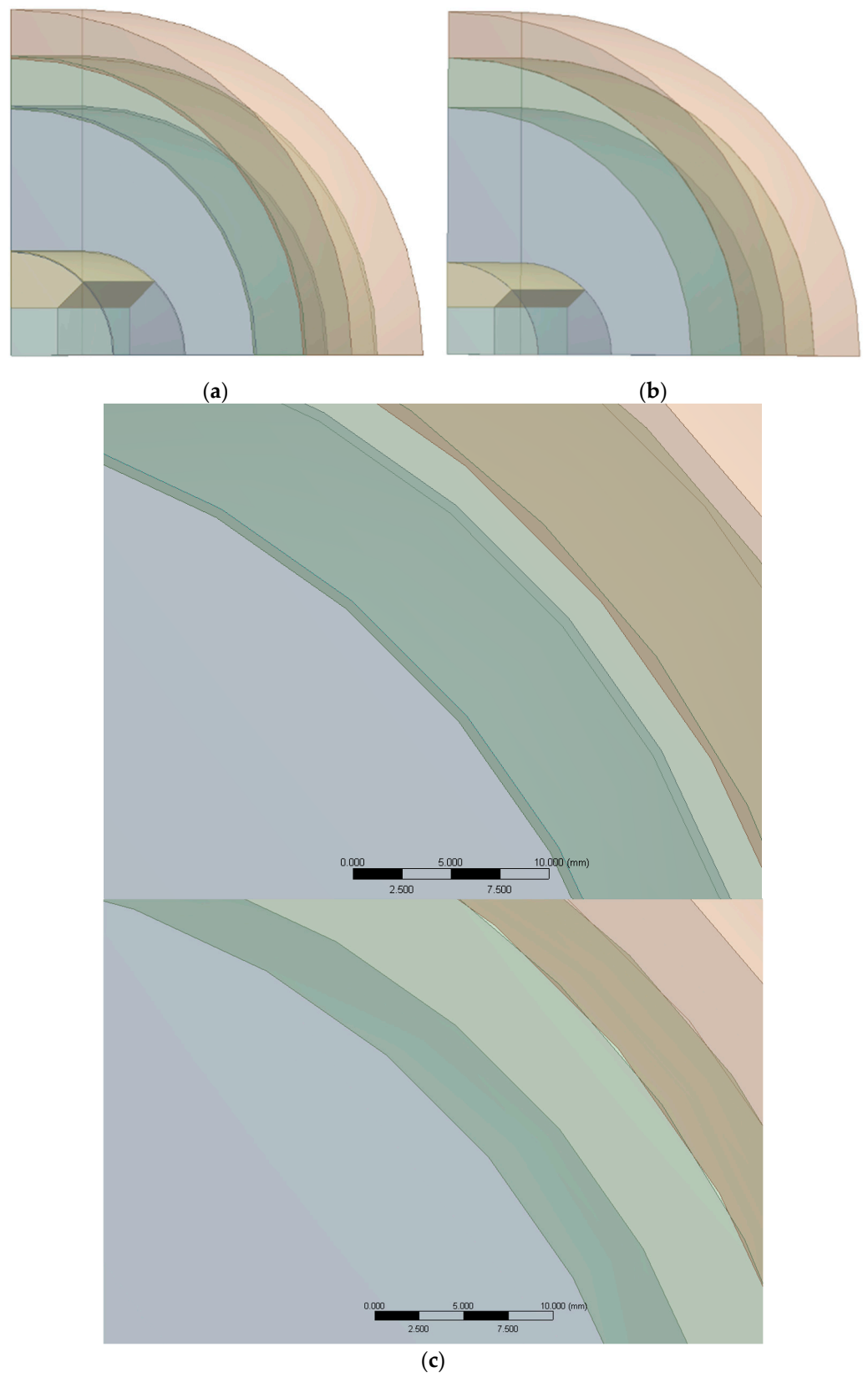


Figure 7. (a) Geometric interference modeling diagram. (b) Contact interference modeling diagram. (c) Comparison of modeling between the two methods.

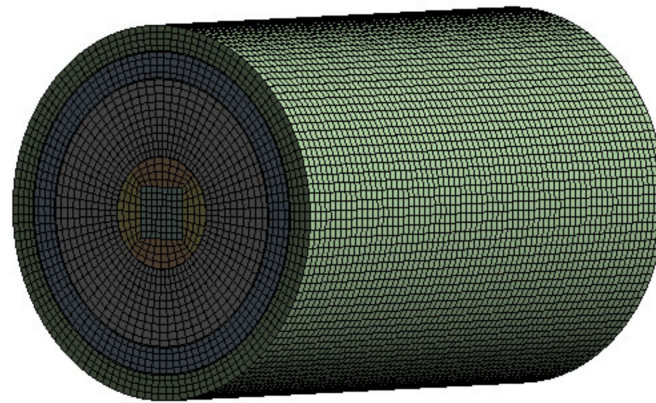


Figure 8. Geometric interference meshing.

3. Results and Analysis

In this experiment, we selected a type of cable with properties as shown in Table 2. Because physical properties of various materials are related to temperature, we considered 20 °C for all the parameters used in all the physical and simulation experiments.

Table 2. Parameters of cable used in experiments.

Number of Layers	Name	Material	Inside Diameter (mm)	Outside Diameter (mm)	Elastic Modulus (GPa)	Poisson's Ratio
1	Conductor	Red copper	-	39.4	109	0.31–0.34
2	Insulator	XLPE	39.4	94	0.7–1.4	0.4
3	Sheath	Aluminum alloy	94	113	70–79	0.33
4	Outer sheath	Polyethylene	113	130.5	0.7–1.4	0.4

3.1. Experiment 1 Test Results and Theoretical Calculations

Experimental results are shown in Figure 9.

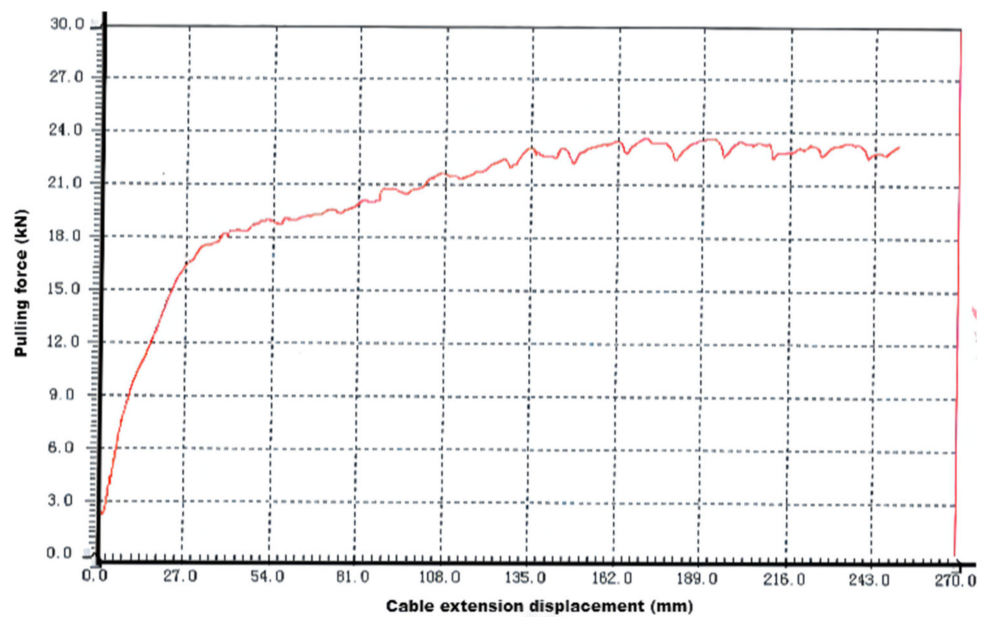


Figure 9. Tensile force–displacement result of Experiment 1. Abscissa represents cable conductor displacement (mm), and ordinate represents applied tensile force (kN).

Experimental results in Figure 9 show that the experimental tensile force was stable at about 23.64 kN, the cable was removed at 135 mm when it was stable for the first time, and

the experimental cable length was 2 m. From Equation (2), we know that frictional force F was balanced with pulling force F_1 :

$$F = F_1 = 23.64 \text{ kN} \tag{14}$$

Friction coefficient f of cross-linked polyethylene and copper was 0.27. Formula (1) shows that the magnitude of positive pressure p is:

$$p = \frac{F}{f} = \frac{23.64}{0.27} \text{ kN} = 87.55 \text{ kN} \tag{15}$$

From Formulas (3) and (15), the interface pressure can be obtained as:

$$\sigma = \frac{p}{A} = \frac{p}{\pi a(L_0 - L)} = \frac{87.55}{\pi \times 39.4 \times (2000 - 135)} \text{ MPa} = 37.925 \text{ MPa} \tag{16}$$

where L_0 is the original length of the experimental cable, and L is the length pulled out after reaching balance.

The direction of the interface pressure points to the center of the conductor cross-section.

The conductor was metallic copper and had a certain linear elasticity. Generally speaking, copper conductors may undergo some deformation during the stretching process, and these deformations may affect the judgment of stretching length [39,40]. In Experiment 1, from the tension–elongation curve, we found that the elongation caused by tension was 135 mm. To avoid the influence of the elastic deformation of the conductor, type variable needed to be calculated according to Hooke’s law:

$$\sigma = E \times \varepsilon \tag{17}$$

where E is the modulus of elasticity (Pa), and ε is the type variable.

Table 1 shows that the elastic modulus of copper was 109 GPa, and the conductor diameter was 39.4 mm according to the calculation formula of axial force

$$\sigma = \frac{F}{S} \tag{18}$$

where F is the tensile force and S is the cross-sectional area.

Combining (17) and (18), the type variable is:

$$\varepsilon = \frac{\sigma}{E} = \frac{F}{E \times S} = \frac{F}{E \times \pi \times \left(\frac{a}{2}\right)^2} = \frac{23.64 \times 10^3}{\pi \times 109 \times 10^9 \times \left(\frac{39.4}{2} \times 10^{-3}\right)^2} \text{ mm} = 0.177 \text{ mm} \tag{19}$$

where a is the radius of the conductor cross-section. From Formula (19), elongation was only 0.177 mm after the cable conductor had been stretched, and this length could be ignored. Therefore, we proved that the tensile amount of the cable in this experiment did not include the length of conductor deformation due to tensile force. The pulling force provided in the experiment only pulled the conductor out.

3.2. Experiment 2 Test Results and Theoretical Calculations

Table 3 shows the actual measured inner and outer diameters of Parts A and B.

Table 3. Comparison between inner and outer diameters measured in Experiment 2 and the reference value.

Number of Layers	Material	Part A Inner Diameter (mm)	Part A Outer Diameter (mm)	Part B Inner Diameter (mm)	Part B Outer Diameter (mm)	Reference Value Inner Diameter (mm)	Reference Value Outer Diameter (mm)
1	Red copper	-	39.41	-	39.41	-	39.4
2	XLPE	39.41	94.42	39.26	95.46	39.4	94
3	Aluminum alloy sheath	94.42	113.2	94.15	114.45	94	113
4	Polyethylene outer sheath	113.2	129.8	112.48	130.28	113	130.5

The actual deformation value can be calculated from Table 3. From the data, we found that the actual measured value of the cable slightly differed from the reference

standard value. Using Equations (6)–(13) again, we calculated the actual deformation, and the internal and external pressure of each layer, as shown in Table 4. We calculated the numerical values in Table 4 by the following method: according to Formulas (6)–(13), because the outermost layer was placed in air without external pressure, external pressure was zero. Then, according to the measured values of the inner and outer diameters, the radial displacement u of the outermost layer could be determined. Then, the value of the internal pressure was calculated according to Formula (13). This value was equal to the value of the inner and outer pressure in the inner layer, and, by analogy, the value of the conductor interface pressure could be obtained.

Table 4. Deformation of each layer of the cable, and calculated internal and external pressure values.

Number of Layers	Material	Internal Pressure (MPa)	External Pressure (MPa)	Deformation Value (mm)
1	Red copper	-	37.54	-
2	XLPE	37.54	21.03	0.69
3	Aluminum alloy sheath	21.03	1.43	1.52
4	Polyethylene outer sheath	1.43	0	1.20

Table 4 shows that conductor interface pressure was 37.54 MPa.

3.3. Simulation Experiment Results by ANSYS

In the contact interference setting, preprocessing does not involve geometric interference, and we modeled and meshed the definition of material properties, and inner and outer diameters using the data in Table 2.

We used cylindrical coordinates and displayed the radial stress (X axis in the Figure 10a represents the radial stress direction, Z represents the axial stress direction, and Y represents the circumferential stress direction). In addition, we arranged all displayed regions as conductor layers. Because the selected target surfaces when setting the solution were all conductor surfaces, only the inner conductors were displayed. After taking the above settings and solving, results were obtained and are shown in Figure 10a,b (unit of interface pressure is marked in each picture (MPa)).

Maximal, minimal, and average values of interface pressure are shown in Table 5. We obtained all data in this section from simulations, and these were not modified. Section 4 reserves two decimal places for calculation purposes.

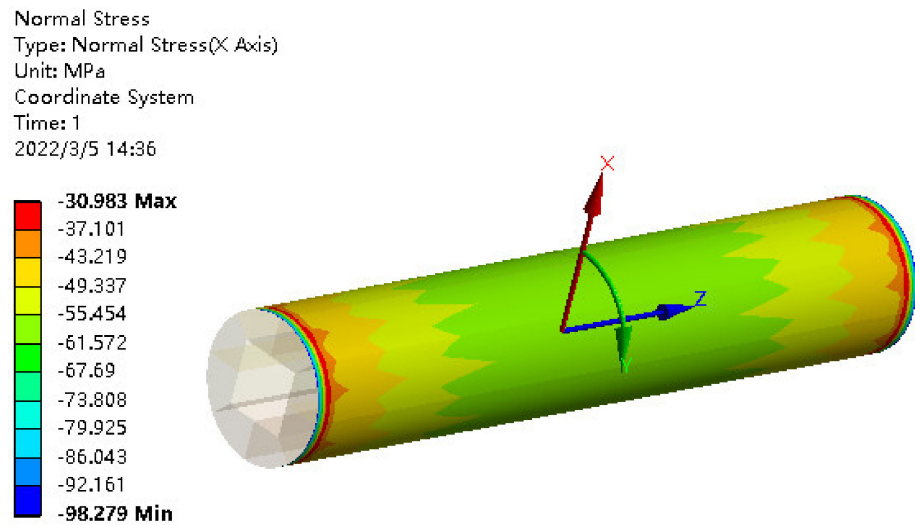
Table 5. Results of geometric interference setting method.

Postprocessing Method	Minimum (MPa)	Maximum (MPa)	Average Value (MPa)
Normal stress	−98.279	−30.983	−55.044
Pressure	27.862	41.805	36.835

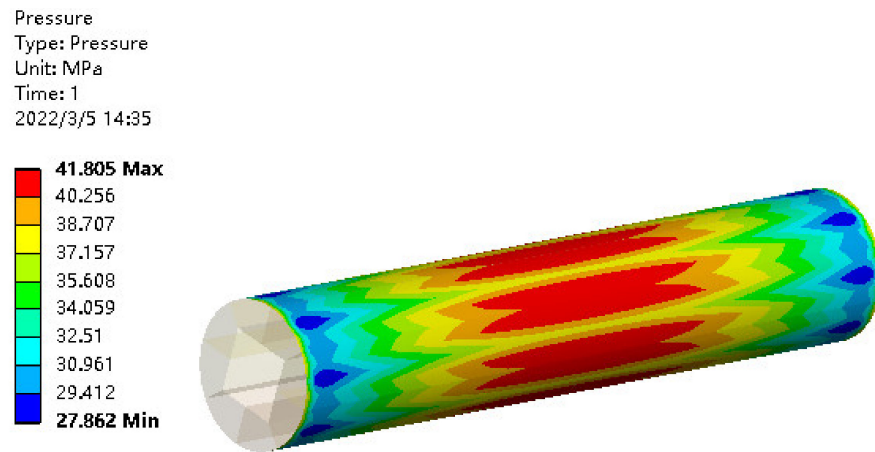
According to Table 5, average stress after the normal stress treatment was −55.044 MPa; the sign is negative because interface pressure on the cable conductor points to the center of the cross-section. Average stress after pressure treatment was 36.835 MPa. Average values in this section and subsequent tables are the averages of interfacial pressure values over the entire surface of the conductor in the model.

In the contact interference setting, preprocessing did not involve the geometric interference method, and we modeled and meshed the material properties and inner and outer diameter data using the data in Table 2.

The postprocessing method was the same as the above setup except for the geometric interference. Results are shown in Figure 11a,b (unit of interface pressure is marked in each picture (MPa)).



(a)



(b)

Figure 10. (a) Normal stress graph of geometric interference; (b) result of geometric interference pressure.

Maximal, minimal, and average values of interface pressure are shown in Table 6.

Table 6. Results of contact interference setting method.

Postprocessing Method	Minimum (MPa)	Maximum (MPa)	Average Value (MPa)
Normal stress	-8.6169	-4.545	-5.7609
Pressure	35.544	37.837	36.568

According to the results of the two simulations in Section 3.3, we found that, when we used the geometric interference method, average stress after normal stress treatment was -39.754 MPa, and average stress after pressure treatment was 36.835 MPa. When using contact interference in the method, average stress after normal stress treatment was -5.7609 MPa, and average stress after pressure treatment was 36.568 MPa.

We compared the simulation and experimental results, and found that the pressure treatment produced results that were the closest to the experimental results.

3.4. Simulation Results from SolidWorks

To further verify the simulation results, we analyzed and verified the simulations in the SolidWorks simulation environment. First, we defined the material properties

(ignoring some structures that did not affect the amount of stress, such as water-blocking and shielding layers) before modeling. The structure was composed of a conductor, cross-linked polyethylene insulation layer, sheath, and polyethylene layer from inside to outside. The material properties were the same as those listed in Table 1, but the inner and outer diameter values were those of Part B in Table 2. We used a quarter-circle model instead of a full cross-section circle. We added a fixed and a symmetry constraint. Because cables under normal placement have no load, mutual force is generated by interference fit. For this reason, we designed a method to calculate the interface pressure using SolidWorks software and established a new model. After the setting had been completed, the model was as shown in Figure 12. Figure 12a shows the model built with SolidWorks, and Figure 12b depicts the meshing. The blue part in Figure 11 is the coordinate system.

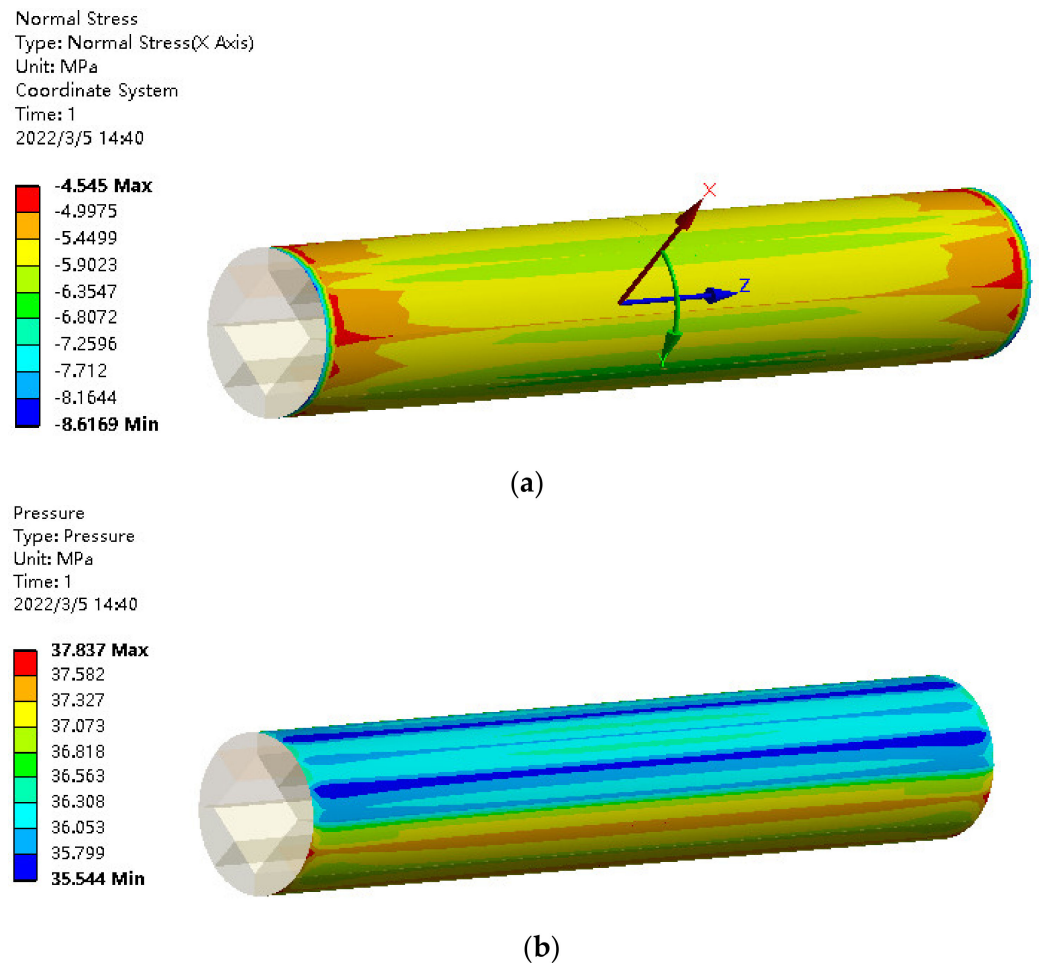


Figure 11. (a) Normal stress graph of contact interference. (b) Contact interference pressure result graph.

The contact pressure diagram is shown in Figure 13a,b. In Figure 13a, the yellow part is the value of the interface pressure between conductor and insulator calculated by the simulation software. Figure 13b shows the X-axis orthogonal stress diagram. The blue part in the middle is the conductor, the outer layer of the conductor is the insulator, and the interface pressure was generated in these two layers (Computer software expressing exponential powers is replaced by the letter E or e).

To more clearly demonstrate the value of the interface pressure on the conductor, we detected the conductor contact surface, as shown in Figure 11. The actual data that we obtained are shown in Figure 12. The abscissa in Figure 14a,b is the node position, and the ordinate is the interface pressure value.

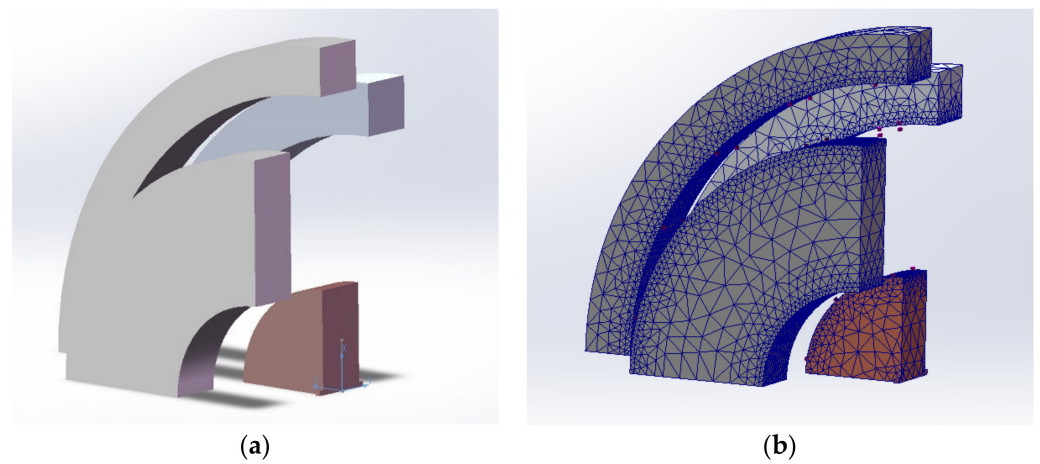


Figure 12. (a) SolidWorks modeling diagram (exploded view). (b) Model meshing.

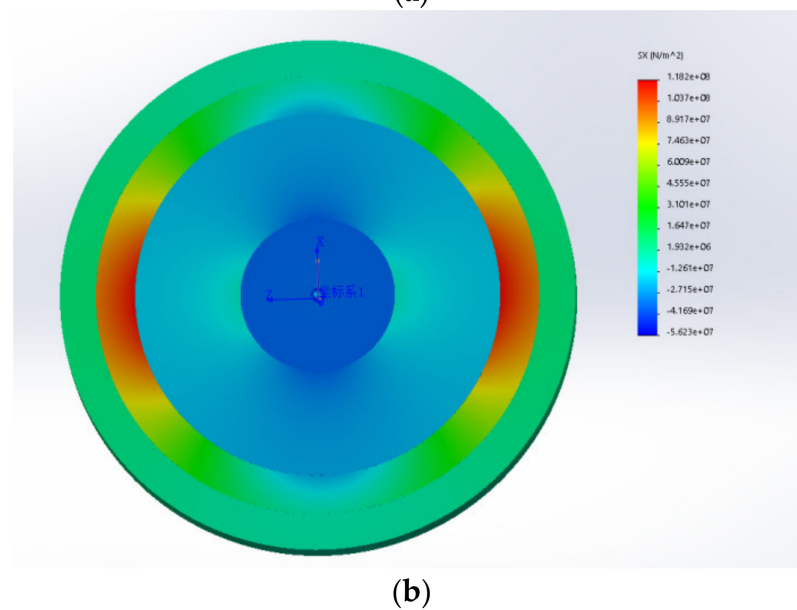
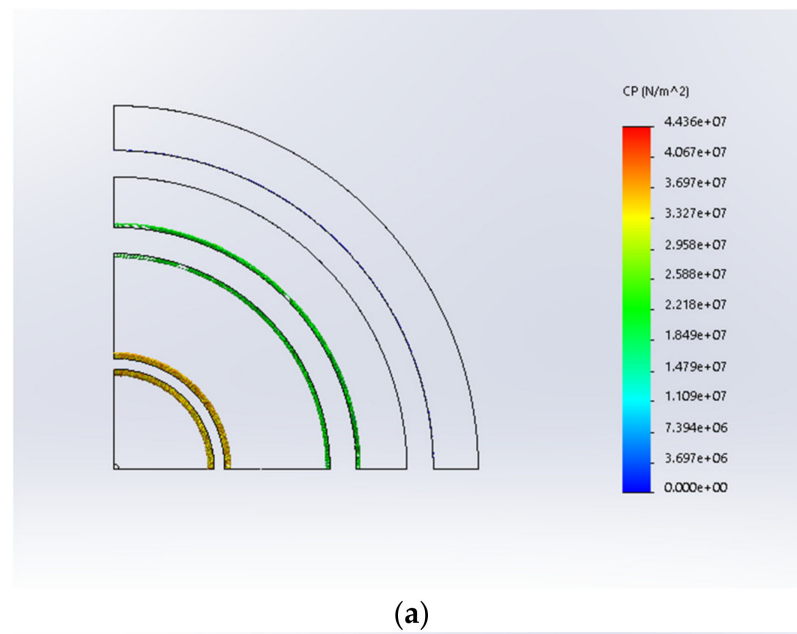


Figure 13. (a) Contact pressure diagram. (b) X-axis orthogonal stress diagram.

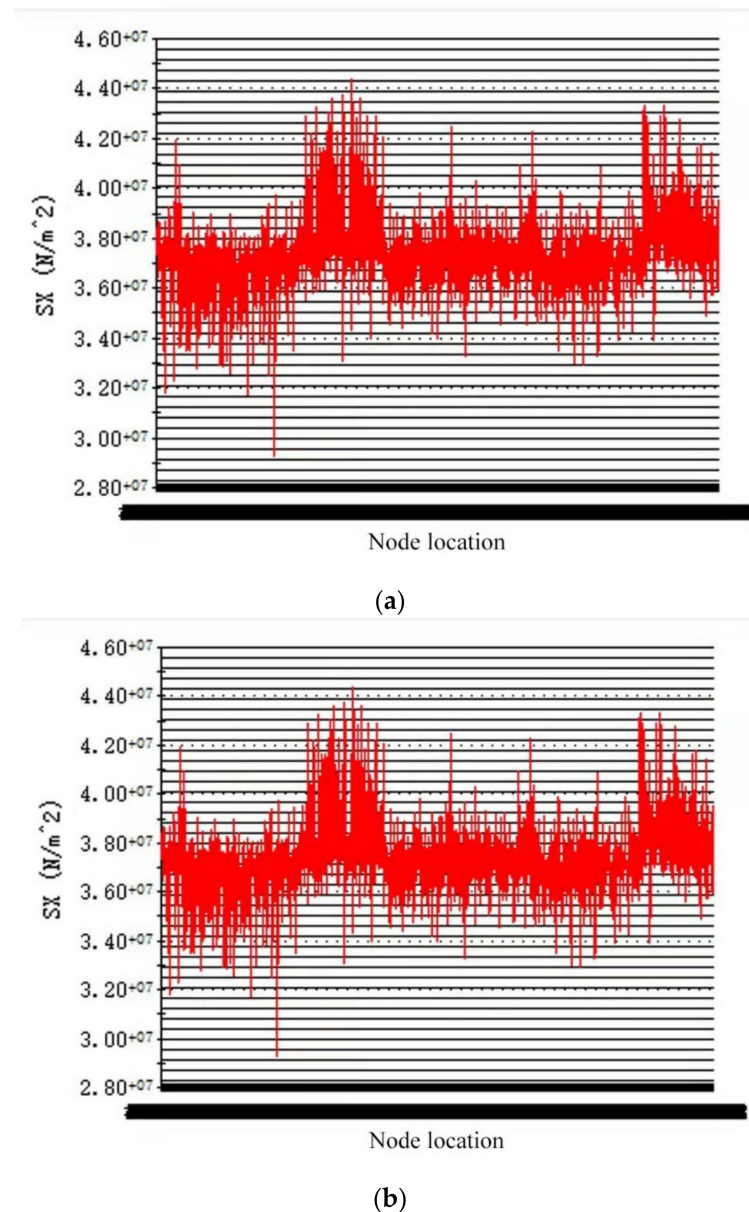


Figure 14. (a) Detection of contact surface of contact pressure conductor. (b) X-axis orthogonal conductor contact surface detection diagram.

The data that we obtained according to the detection results are shown in Table 7.

Table 7. SolidWorks simulation data table.

Approach	Minimum (MPa)	Maximum (MPa)	Average Value (MPa)
Contact stress method	29.25	44.36	37.36
X-axis orthogonal stress method	−44.4	−30.33	−37.36

Table 7 shows that we used the average value obtained by the contact stress method and the X-axis orthogonal stress method to obtain a conductor interface pressure of 37.36 MPa. In the simulation experiments using ANSYS Workbench and SolidWorks, the results obtained are expressed as average values. Results show that those obtained by the X-axis orthogonal stress method in the SolidWorks simulation were the closest to the physical experimental value, which was 37.37 MPa.

4. Discussion

We provide the results of Experiments 1 and 2, ANSYS Workbench simulation, and SolidWorks simulation in Tables 8 and 9.

Table 8. Calculated interface pressure gauge for Experiments 1 and 2.

Experiment	Experiment 1	Experiment 2
Calculation results (MPa)	37.925	37.54

Table 9. Statistics of simulation results.

Approach	Minimum (MPa)	Maximum (MPa)	Average Value (MPa)
Geometric interference normal stress	30.98	98.28	55.04
Geometric interference pressure	27.86	41.81	36.84
Contact interference normal stress	8.62	4.55	5.761
Contact interference pressure	35.54	37.84	36.57
Contact stress method	29.25	44.36	37.36
X-axis orthogonal stress method	44.4	30.33	37.36

The statistics of the simulation results are shown in Table 9, and results are all absolute values.

Table 9 shows that, using ANSYS Workbench processing, the cable conductor interface pressure values obtained by the geometric interference setting were 39.75 and 36.84 MPa; values obtained by the contact setting should be 5.76 and 36.57 MPa. The cable SolidWorks simulation obtained a conductor interface pressure value of 37.36 MPa. Taking the value from Experiment 1 as the reference standard, we calculated the error of the average simulation value; results are shown in Table 10.

Table 10. Experiment 1 and simulation value error.

Experimental Method	Experiment 1	Geometric Interference Normal Stress	Geometric Interference Pressure	Contact Interference Normal Stress	Contact Interference Pressure	Contact Stress	X-axis Orthogonal Stress
Experimental value (MPa)	37.93	55.04	36.84	5.76	36.57	37.36	37.36
Error	0	45.1%	2.87%	84.8%	3.59%	1.50%	1.50%

Table 10 shows that the minimal error between the value obtained using SolidWorks simulation and Experiment 1 was 1.5%, and the maximal error generated using ANSYS Workbench contact interference normal stress was 84.8%. When using the two postprocessing methods in SolidWorks, as shown in Table 6, we found that the interface pressure value range obtained by the X-axis orthogonal method was the smallest, and the values were close to the experimental values.

When we used the value of Experiment 2 as the standard, we calculated the error calculation with the average simulation value; the results are shown in Table 11.

Table 11. Experiment 2 and simulation value error.

Experimental Method	Experiment 2	Geometric Interference Normal Stress	Geometric Interference Pressure	Contact Interference Normal Stress	Contact Interference Pressure	Contact Stress	X-axis Orthogonal Stress
Experimental value (MPa)	37.54	55.04	36.84	5.76	36.57	37.36	37.36
error	0	46.4%	1.86%	84.7%	2.58%	0.48%	0.48%

Table 11 shows that the minimal error between the value obtained using SolidWorks simulation and Experiment 2 was 0.48%, and the maximal error generated using ANSYS Workbench contact interference normal stress was 84.7%. When using the two postprocessing methods in SolidWorks, Table 6 shows that the interface pressure value range obtained by the X-axis orthogonal method was the smallest, and the X-axis orthogonal method was the most accurate.

Results show that the calculated interface pressure of the cable conductor was 37.93 MPa in Experiment 1, and the interface pressure of the cable conductor was 37.54 MPa in Experiment 2. Interface pressure values obtained using the two different methods were similar; simulation results show that the interface pressure value obtained by the geometric interference normal stress method was 39.75 and 36.84 MPa with the geometric interference pressure method, 5.76 MPa with the contact interference normal stress method, 36.57 MPa with the contact interference pressure method, 37.36 MPa with the contact stress method, and 37.36 MPa by the X-axis orthogonal stress method. The comparison shows that the X-axis orthogonal stress method was the most accurate, with errors of 1.5% and 0.48% compared with Experiment 1 and 2 values, respectively.

Tables 10 and 11 show that some of the simulation setting methods are reliable, and their error is small. However, for the contact interference normal stress method, the error was more than 80%, indicating that this method of analyzing the pressure of the cable interface is unsuitable under these settings.

5. Conclusions

Addressing the problem of the difficulty in calculating and analyzing cable conductor interface pressure, we constructed a new calculation and measurement experiment method in this study as follows.

On the basis of Coulomb's friction law and the force balance theorem, we proposed a calculation and experimental method for determining the interface pressure of cable conductors by measuring friction force between cable conductors and insulators. The method was described in Experiment 1. The method of Experiment 1 was verified and was reliable. Friction force is generated after the cable conductor is pulled. Positive pressure is obtained through friction force, and interface pressure is then solved. We used the method in Experiment 1 to obtain the interface pressure of the cable, which was 37.93 MPa. On the basis of the elastic mechanics formula, we designed a method to obtain the interface pressure on the conductor by calculating the deformation value of each layer of the cable before and after stripping, and we verified the accuracy of the method through experiments. As shown by Experiment 2, the final conductor interface pressure was 37.54 MPa. By using ANSYS and SolidWorks simulation software, we built a corresponding cable model. We used geometric interference setting, contact interference setting, contact stress setting, and X-axis orthogonal stress setting to simulate the interface pressure. On the basis of the experimental results of the two methods, we calculated the errors of simulation and experimental benchmark results, and conducted a comparative analysis. Results show that the SolidWorks X-axis orthogonal stress method was the most accurate: interface pressure was 37.36 MPa, and errors were 1.5% and 0.48% in Experiments 1 and 2, respectively.

In this experiment, two physical experiments were proposed and verified. However, in the process of Experiment 2, the measurement of Part B could also become more accurate. In follow-up research, after measuring the interface pressure of the cable conductor, the interface pressure of the cable conductor in different states during construction can be studied further.

Author Contributions: Conceptualization, C.L., S.W., S.L. and Y.G.; methodology, C.L., S.W., S.L. and Y.G.; software, S.W.; validation, S.L. and C.L.; formal analysis, C.L., S.W. and S.L.; resources, S.L., S.W., C.L., and Y.G.; data curation, S.L., C.L., S.W. and Y.G.; writing—original draft preparation, S.L., C.L. and S.W.; writing—review and editing, S.L., C.L. and S.W.; visualization, S.L., C.L. and S.W.; supervision, C.L.; project administration, C.L., S.L. and Y.G. All authors have read and agreed to the published version of the manuscript.

Funding: This work was supported by the Fishery Administration Project (D8021210076). The funders had no role in study design, data collection, or analysis; the decision to publish; or the preparation of the manuscript.

Informed Consent Statement: Informed consent was obtained from all subjects involved in the study.

Data Availability Statement: Data were obtained from the experimental and simulation software designed in this study, which we obtained by rigorous calculation and logical reasoning.

Acknowledgments: We thank the project side for the use of the site and equipment required for the experiment in this study.

Conflicts of Interest: The authors declare no conflict of interest.

References

1. Sun, J.; Xu, X. History of electrical power cables. In *Electrical Power Cable Engineering*, 3rd ed.; Chenggui, F., Ed.; China Machine Press: Beijing, China, 2014; pp. 1–10.
2. Lu, Y.; Liu, C.; Meng, S. Stress Analysis of Bended State Aluminum Cable Steel Reinforced Conductor. *J. China Three Gorges Univ.* **2018**, *40*, 4.
3. Zhou, X.; Qu, C.; Liu, S. Simulation analysis on mechanical properties of aluminum cable steel reinforced under tensile load. *J. Graph.* **2020**, *41*, 7.
4. Luo, Y.; Han, Z.; Zhou, M.; Wang, H. A Sophisticated Method of the Mechanical Design of Cable Accessories Focusing on Interface Contact Pressure. *Energies* **2020**, *13*, 2976. [[CrossRef](#)]
5. Chen, J.; Hu, L.; Liu, Y. Study on Interface Pressure Measurement of Cable Connector Based on Piezoelectric Sensor. *Piezoelectrics Acousto-optics* **2021**, *43*, 5.
6. Jia, Z.; Zhang, Y.; Fan, W.; Zhu, B.; You, J. Analysis of the Interface Pressure of Cold Shrinkable Joint of 10 kV XLPE Cable. *High Volt. Eng.* **2017**, *43*, 5.
7. Qiu, W.; Li, Y.; Cui, J. Effect Rule of Cable Bending on Interface Pressure Inside Cable Joint. *Insul. Mater.* **2020**, *53*, 7.
8. Tian, Z.; Liying, S.; Xiaoye, B. Research on the Method of Measuring the Interface Pressure of Prefabri-cated Cable Joint Based on Finite Element Analysis. *Electr. Wire Cable* **2019**, *4*, 173–176.
9. Tian, Z.; Sun, L.; Bai, X. A Study of Simulation on Relationship Between Young’s Modulus of Cable joints and Interface Pressure Based on Finite Element Method. *J. Phys. Conf. Ser.* **2019**, *2019*, 22–36. [[CrossRef](#)]
10. Zhang, D.; Han, Y.; Liu, H. Determination of the Pressure Distribution at the XLPE Ca-ble-rubber Interface in a Self-pressurized Joint. *High Volt. Eng.* **2007**, *33*, 4.
11. Mohammad, A.H.; Pilgrim, J.; Lewin, P. Thermo-mechanical analysis of solid interfaces in HVAC cable joints. *IEEE Trans. Dielectr. Electr. Insul.* **2019**, *26*, 1779–1787.
12. Di Sante, R.; Ghaderi, A.; Mingotti, A.; Peretto, L.; Tinarelli, R. Effects of Thermal Cycles on Interfacial Pressure in MV Cable Joints. *Sensors* **2019**, *20*, 169. [[CrossRef](#)] [[PubMed](#)]
13. Bao, S.; Deng, H.; Han, Z. The influence of aging cable insulation on the interface pressure of cable joint. *Electr. Power Eng. Technol.* **2020**, 16–22.
14. Castro-Fresno, D.; Diaz, J.; López, L.; Nieto, P. Evaluation of the resistant capacity of cable nets using the finite element method and experimental validation. *Eng. Geol.* **2008**, *100*, 1–10. [[CrossRef](#)]
15. Cui, J.; Dong, Y.U.; Wang, X.; Qiu, W.; Huang, S.; Wei, Y. Research Progress of Measuring Method for Interface Pressure Between Cable and Accessory. *Insul. Mater.* **2018**, *51*, 6.
16. Sun, T.; Zhang, Y.; Guo, X. Partial discharge behavior of 220 kV prefabricated cable termination induced by inadequate interface pressure. In Proceedings of the 2018 12th International Conference on the Properties and Applications of Dielectric Materials (ICPADM), Xi’an, China, 20 May 2018.
17. Di, A.; Hm, B.; Pcha, C.; Ss, A. Experimental and analytical study on the mechanical behaviour of cable bolts subjected to axial loading and constant normal stiffness. *Int. J. Rock Mech. Min. Sci.* **2019**, *113*, 83–91.
18. Liao, Y.; Bao, S.; Xie, Y.; Zhao, Y.; Xu, Y. Breakdown failure analysis of 220 kV cable joint with large expanding rate under closing overvoltage. *Eng. Fail. Anal.* **2020**, *120*, 105086. [[CrossRef](#)]
19. Yu, Z.; Shao, S.; Liu, N.; Zhou, Z.; Feng, L.; Du, P.; Tang, J. Cable tension identification based on near field radiated acoustic pressure signal. *Measurement* **2021**, *178*, 109354. [[CrossRef](#)]
20. Liang, B. Analysis of the Production of 110kV and above Cross-linked Cable Joints. *Audio Eng.* **2018**, *42*, 3.
21. Zhao, H.; Zhou, C. The Design of High-Voltage and Extra-High Voltage XLPE Power Cable Outdoor Termination. *Wire Cable* **2021**, *2*, 33–35.
22. Zhao, L.; Qiu, J.; Li, Y.; Ren, J.; Jia, L.; Wang, Z. Interface Pressure Evolution Law of Cable Intermediate Joint Under Silicone Grease Environment. *Insul. Mater.* **2021**, *54*, 5.
23. Li, W.; Zhu, K.; Deng, Y. Influence of Temperature on Initiation Mechanism of Partial Discharge at the Interface Defects of Cable Accessories. *Electr. Power* **2021**, *54*, 9.
24. Liang, H. Research on the main problems in the design of high-voltage cable accessories. *Low Carbon World* **2019**, *9*, 2.

25. Xu, D.P.; Jiang, Q.; Li, S.; Qiu, S.; Huang, S.L. Safety assessment of cable bolts subjected to tensile loads. *Comput. Geotech.* **2020**, *128*, 103832. [[CrossRef](#)]
26. Sun, F.; Yang, S.; Bai, S.; Wang, Q. Reuse of Pan-milled P-XLPE cable powder as additive for asphalt to improve thermal stability and decrease processing viscosity. *Constr. Build. Mater.* **2021**, *281*, 122593. [[CrossRef](#)]
27. Ez, A.; Km, A.; Mta, B. Water trees in polyethylene insulated power cables: Approach to water trees initiation mechanism. *Electr. Power Syst. Res.* **2019**, *180*, 106158.
28. Zhou, K.; Yuan, H.; Akram, S.; Meng, P.; Mahmood, A.; Aamir, M.; Imran, M. Healing of water tree aged cables using rejuvenation nanofluid. *Polym. Test.* **2021**, *102*, 107324. [[CrossRef](#)]
29. Li, K.; Xie, Z.; Zeng, D.; Li, W.; Xia, C. Power cable vibration monitoring based on wireless distributed sensor network. *Procedia Comput. Sci.* **2021**, *183*, 401–411. [[CrossRef](#)]
30. Xia, Z.; Yao, Q.; Xu, Q.; Ma, J.; Liu, Z. Numerical-modeling-based assessment of the impact of two-end-type cable support on failure characteristics of yield pillars. *Eng. Fail. Anal.* **2021**, *128*, 105619. [[CrossRef](#)]
31. Lai, Q.; Chen, J.; Hu, L.; Cao, J.; Zhu, N. Investigation of tail pipe breakdown incident for 110 kV cable termination and proposal of fault prevention. *Eng. Fail. Anal.* **2020**, *108*, 104353. [[CrossRef](#)]
32. Zhu, C.; Zhuang, Y.; Chen, Y.; Zhang, B.; Huang, J. Contactless liquid interface measurement based on a hollow coaxial cable resonator. *Sens. Actuators A Phys.* **2019**, *285*, 623–627. [[CrossRef](#)]
33. Pompili, M.; Calcara, L.; D’Orazio, L.; Ricci, D.; He, H. Joints defectiveness of MV underground cable and the effects on the distribution system. *Electr. Power Syst. Res.* **2021**, *192*, 107004. [[CrossRef](#)]
34. Ar, A.; Mae, B.; Ias, B.; Mas, A.; Mk, A. Failure analysis of articulated paddings at crossing interface between crossing cable and crossed pipeline. *Appl. Ocean. Res.* **2021**, *115*, 102850.
35. Viespoli, L.M.; Panza, L.; Johanson, A.; Alvaro, A.; Berto, F. Tape winding angle influence on subsea cable sheathing fatigue performance. *Eng. Struct.* **2021**, *229*, 111660. [[CrossRef](#)]
36. Zan, Y.; Guo, R.; Xue, Y.; Bai, X.; Liu, P.; Huang, F. Experimental and numerical investigations of regular head wave effects on cable tension of a subsea module during lowering operations. *Ocean. Eng.* **2021**, *239*, 109822. [[CrossRef](#)]
37. Nejad, M.Z.; Jabbari, M.; Ghannad, M. Elastic Analysis of Rotating Thick Cylindrical Pressure Vessels under Non-Uniform Pressure: Linear and Non-Linear Thickness. *Period. Polytech. Mech. Eng.* **2015**, *59*, 65–73. [[CrossRef](#)]
38. Abdalla, H.; Casagrande, D.; Bona, F.D. A Dynamic Programming Setting for Functionally Graded Thick-Walled Cylinders. *Materials* **2020**, *13*, 3988. [[CrossRef](#)]
39. Lizheng, Q. *Experimental and Simulation Study on Tensile Properties of Metallic Materials Characterized by Continuous Ball Indentation Technique*; Shanghai Jiao Tong University: Shanghai, China, 2019.
40. Bosiakov, S.; Trzepieciniski, T. Analysis of Frictional Resistance Arising at the Edge of the Sheet Metal Drawing Die. *J. Frict. Wear* **2019**, *40*, 151–155. [[CrossRef](#)]